EPiC Series in Engineering
Volume 5, 2023, Pages 50–60
Proceedings of International Symposium on Applied Science 2022

Thermo-stress analysis in two-dimensional Functionally Graded Materials by a meshfree Radial Point Interpolation Method

Van Long Hoang[1,2], My Hien Nguyen Thi[3] and Thanh Nha Nguyen[1,2*]
[1] Department of Engineering Mechanics, Faculty of Applied Sciences, Ho Chi Minh City University of Technology (HCMUT), 268 Ly Thuong Kiet Street, District 10, Ho Chi Minh City, Viet Nam
[2] Vietnam National University Ho Chi Minh City, Linh Trung Ward, Thu Duc City, Ho Chi Minh City, Viet Nam
[3]Institute of Transport and Environment Research, Ho Chi Minh City University of Transport, 2 Vo Oanh Street, Ward 25, Binh Thanh District, Ho Chi Minh City, Vietnam.
nhanguyen@hcmut.edu.vn

Abstract

Functionally graded materials (FGMs) are advanced composites whose properties are continuously variable according to their dimensions in one or more predefined directions. The application range of this material is becoming wider and wider, therefore, studies on the activity of functionally graded materials (FGMs) in high-temperature environments become more and more important and necessary. In this study, a mesh-free Radial Point Interpolation Method (RPIM) has been proposed to solve a coupled thermo-mechanical problem in functionally graded metal/ceramic plates. The most important advantage of this method is that the shape functions satisfy the property of Kronecker's delta function. Thus the essential boundary conditions are easily implemented as in the finite element method (FEM). The obtained results are compared with the reference ones from analytical solutions and finite element methods by commercial software COMSOL Multiphysics to verify the effectiveness and reliability of this method.

1 Introduction

Functionally graded materials (FGM) are new composites designed for specific applications, especially in engineering structures in high temperature environments. Functional Graded Materials (FGM) are usually composed of two or more different materials, in which the volume fractions of the

* Corresponding author

materials are smoothly and continuously changed in the desired directions. The application of FGM have become much more widespread and popularization as structural components in transportation, energy, electronics and biomedical engineering, etc. Therefore, thermomechanical behaviors in FGM materials have been extensively studied over the past few decades with numerical simulation techniques. Many numerical methods have been developed and improved to make numerical simulations easier and more efficient. Among them, the finite element method (FEM), see [1,2] and references therein, is still a method with a long history of development and is the most popular tool to support numerical simulation. However, there are certain disadvantages. A meshless method has been developed to overcome those disadvantages [3-5]. However, most of the meshless methods do not possess the properties Kronecker's delta function like the FEM, leading to difficulties in treatment of boundary conditions.

In this paper, the author uses a point interpolation meshless method based on radial basis functions to analyzed stresses for functionally graded material plates under combined thermomechanical loads. The most important advantage of this method is that the shape functions satisfy the Kronecker's delta property. Until now, RPIM has been widely applied in solving mechanical problems. For example, "A Meshfree Radial Point Interpolation Method for Free Vibration of Laminated Composite Plates Analysis Based on Layerwise Theory" [6], "Meshfree radial point interpolation method for analysis of viscoplastic problems" [7], "A meshfree radial point interpolation method (RPIM) for three-dimensional solids" [8], "An Improved 2D Meshfree Radial Point Interpolation Method for Stress Concentration Evaluation of Welded Component" [9], etc.

2 RPIM Shape Function

The Radial Point Interpolation method (RPIM) is presented in order to build the shape functions and its derivatives. The domain influence is represented by a set of arbitrarily distributed nodes in the problem domain and its boundary. The approximation function $u(\mathbf{x})$ at a point of interest x with a set of arbitrarily distributed nodes using radial basis function $R_i(\mathbf{x})$ augmented with polynomial basis function $P_j(\mathbf{x})$ can be written as:

$$u(\mathbf{x}) = \sum_{i=1}^{n} R_i(x)a_i + \sum_{j=1}^{m} P_j(x)b_j = \left[\mathbf{R}^T(\mathbf{x})\mathbf{A} + \mathbf{P}^T(\mathbf{x})\mathbf{B}\right]\mathbf{U}_s \tag{1}$$

where n is the number radial basis functions (RBFs) and m is the number of polynomial basis functions, $\mathbf{R}(\mathbf{x})$ and $\mathbf{P}(\mathbf{x})$ are radial and polynomial basis functions, respectively. Matrix **A**, **B** and matrices in which can be seen detail in [10]. Vectors $\mathbf{R}(\mathbf{x})$ and $\mathbf{P}(\mathbf{x})$ is defined by

$$\mathbf{R}^T(\mathbf{x}) = \left\{R(\mathbf{x}_1, \mathbf{x}) \quad R(\mathbf{x}_2, \mathbf{x}) \quad ... \quad R(\mathbf{x}_n, \mathbf{x})\right\} \tag{2}$$

$$\mathbf{P}^T(\mathbf{x}) = \left\{P(\mathbf{x}_1) \quad P(\mathbf{x}_2) \quad ... \quad P(\mathbf{x}_m)\right\} \tag{3}$$

where $R(\mathbf{x}_i, \mathbf{x})$ is the correlation function representing the distance between the point of interest **x** and the nodes $\mathbf{x}_i$ ($i \in [1, n]$) of the local support domain. There are four types of radial basic functions (RBFs) presented in [10]. However, in this paper there is only one type used by the author, which is Thin Plate Spline (TPS) function with a single dimensionless parameter given by:

$$R(\mathbf{x}, \mathbf{y}) = r_i^{\eta} \tag{4}$$

where $r_i = \sqrt{(x - x_i)^2 + (y - y_i)^2}$ is a distance between the point of interest **x** and the node $\mathbf{x}_i(x,y)$.

We can rewrite Eq. (1) as follows

$$u(\mathbf{x}) = \mathbf{\Phi}^T(\mathbf{x})\mathbf{U}_s = \sum_{i=1}^{n} \Phi_i u_i \tag{5}$$

where the matrix of shape functions $\mathbf{\Phi}(\mathbf{x})$, see details in [10].

3 Thermomechanical problems for FGM

Let an object be the set of material points of a continuously inhomogeneous isotropic body occupying a 2D domain, which consists of the material area $\Omega \in \mathbb{R}^2$ and its boundary line $\Gamma \in \mathbb{R}^2$. The body is subjected to a traction $\bar{\mathbf{t}}$ on Γ_t, heat flux $\bar{q}$ on Γ_q, prescribed body force $\mathbf{b} = [b_x \quad b_y]^T$ and heat source $\mathbf{Q}$ in the support domain Ω_x. The governing equations for static thermoelastic problem are given by:

$$-\nabla.\mathbf{q} + Q = 0, \tag{6}$$

$$\nabla.\boldsymbol{\sigma} + \mathbf{b} = \mathbf{0}, \tag{7}$$

The heat flux $\mathbf{q}$ related to the temperature gradient is expressed as

$$\mathbf{q} = -k(\mathbf{x})\nabla T, \tag{8}$$

where T is the temperature and $k(\mathbf{x})$ denotes thermal conductivity of the function graded materials. The variable $\mathbf{x}$ denotes the physical dimensions expressed in Cartesian coordinates, $\mathbf{x}$: (x, y).

The relationship between the Cauchy stress tensor $\boldsymbol{\sigma}$ and strain tensor $\boldsymbol{\varepsilon}$ is defined through the generalized Hooke's law as

$$\boldsymbol{\sigma} = \mathbf{C} : (\boldsymbol{\varepsilon} - \boldsymbol{\varepsilon}_T), \tag{9}$$

where $\mathbf{C}$ is fourth-order tensor, $\boldsymbol{\varepsilon}$ is the tensor strain is defined by the gradient of dispalcemant and $\boldsymbol{\varepsilon}_T$ is thermal strain tensor is computed by the difference between the current (calculater by RPIM) and uniform reference temperature T_{ref}. Those tensors are expressed as

$$\boldsymbol{\varepsilon} = \frac{1}{2}\left(\nabla\mathbf{u} + (\nabla\mathbf{u})^T\right) \text{ and } \boldsymbol{\varepsilon}_T = \alpha(\mathbf{x})(T - T_{ref})\mathbf{I}, \tag{10}$$

where $\alpha(\mathbf{x})$ is the function that represents the coefficient of thermal expansion in space coordinates $\mathbf{x}$ and $\mathbf{I}$ is identity second-order tensor.

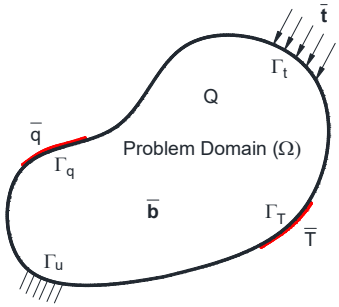

Figure 1: Geometric representation of a thermo-mechanical model and its boundary conditions.

The Dirichlet and Neumann boundary conditions as shown in Fig. 1 are given by

$$T(\mathbf{x}) = \bar{T} \text{ on } \Gamma_T \tag{11}$$

$$\mathbf{q}.\mathbf{n} = \bar{q} \text{ on } \Gamma_q \tag{12}$$

$$\mathbf{q}.\mathbf{n} = h(T - T_\infty) \text{ on } \Gamma_C \tag{13}$$

$$\mathbf{u} = \bar{\mathbf{u}} \text{ on } \Gamma_u \tag{14}$$

$$\boldsymbol{\sigma}.\mathbf{n} = \bar{\mathbf{t}} \text{ on } \Gamma_t \tag{15}$$

where $\bar{\mathbf{u}}$ and $\bar{\mathbf{t}}$ denoting the prescribed displacements on the Dirichlet boundary and the prescribed tractions on the Neumann boundary, respectively, h is the convection coefficient, T_∞ is a temperature in convection and $\mathbf{n}$ is the outward surface normal.

The Galerkin weak forms for coupling thermo-elastic problem for the heat transfer and elastic equations are:

$$\int_{\Omega} k.\nabla T.\nabla(\delta T)d\Omega + \int_{\Gamma_C} \delta T.h.T d\Gamma = \int_{\Omega} Q.\delta T d\Omega + \int_{\Gamma_q} \bar{q}.\delta T d\Gamma + \int_{\Gamma_C} \delta T.h.T_{\infty} d\Gamma \tag{16}$$

$$\int_{\Omega} (\mathbf{C} : \boldsymbol{\varepsilon}) : \delta\boldsymbol{\varepsilon} d\Omega = \int_{\Omega} \mathbf{b}.\delta\mathbf{u} d\Omega + \int_{\Gamma_t} \bar{\mathbf{t}}.\delta\mathbf{u} d\Gamma + \int_{\Omega} (\mathbf{C} : \boldsymbol{\varepsilon}_T) : \delta\boldsymbol{\varepsilon} d\Omega \tag{17}$$

where $\delta\mathbf{u}$ and δT is the virtual displacement and virtual temperature fields that used as a test function, $\mathbf{C}$ is the matrix of elastic constants, for FGM, $\mathbf{C}$ is the function of space coordinates $\mathbf{x}$, assumed different values for the two cases of plane stress and plane strain, see [11].

The system of the variational Eqs. (16) and (17) show that the combined thermomechanical problem is perfectly suitable to be solved using RPIM. In each local support domain, the components of the displacement vector and the temperature change as Eq. (18) are approximated by suitable interpolation functions as follows

$$\mathbf{u}(\mathbf{x}) = \sum_{i=1}^{n} \Phi_i u_i = \boldsymbol{\Phi}_u \mathbf{u}^e, \quad T(\mathbf{x}) = \sum_{i=1}^{n} \Phi_i T_i = \boldsymbol{\Phi}_\theta \mathbf{T}^e \tag{18}$$

where $\mathbf{u}^e$ and $\mathbf{T}^e$ are the node displacement vectors and the temperature at the node in the local support domain, respectively.

The expressions in Eq. (16) and (17) can be rewritten in matrix form as follows:

$$\begin{bmatrix} \mathbf{K}_{uu} & \mathbf{K}_{uT} \\ 0 & \mathbf{K}_{TT} \end{bmatrix} \begin{bmatrix} \mathbf{u} \\ \mathbf{T} \end{bmatrix} = \begin{bmatrix} \mathbf{F}_{uu} \\ \mathbf{F}_{TT} \end{bmatrix} \tag{19}$$

where $\mathbf{K}_{uu}$ and $\mathbf{K}_{TT}$ is usual global stiffness and thermal conductivity matrices, $\mathbf{K}_{uT}$ is coupling matrices combining the mechanical and thermal parts, $\mathbf{u}$ and $\mathbf{T}$ are global vectors of nodal displacements and nodal temperature, respectively. The vectors $\mathbf{F}_{uu}$ and $\mathbf{F}_{TT}$ are global vectors of mechanical and thermal forces. Their detailed forms can be found in [12].

4 Results and discussions

4.1 Functionally graded rectangular plate

In this first example, a steady state thermoelasticity analysis of a FGM plate shown in Fig. 2 is carried out evaluate the performance of the present method with thermomechanical problems. A closed-form solution of this problem is available in [13]. Plate was assumed an exponential variation of Young's modulus, thermal conductivity along the width of the plate. They are defined as the following functions of the x-coordinate [14].

$$V(x) = V_1 e^{\gamma x}, \text{ where } \gamma = \frac{1}{w} \ln\left(\frac{V_2}{V_1}\right) \tag{20}$$

where V_1 and V_2 represent material parameters given on the sides of FGM plate at x = 0 and x = w, respectively, as shown in Table 1.

A FGM rectangular plate with dimensions of w = 1m and L = 2m with the boundary displacements are prescribed on the bottom edge as shown in Fig. 2. Uniform tension $\sigma_0 = 1\text{GPa}$ are applied to the top edge perpendicular to the functionally graded plate, while temperature are applied to the left and right edge with $T_1 = T(x=0) = 100\text{K}$ and $T_2 = T(x=w) = 200\text{K}$, respectively. General expressions of the steady state temperature field T(x) and the respective thermoelastic-induced stress $\sigma_{yy}(x)$ for functionally graded materialscan be found in [13].

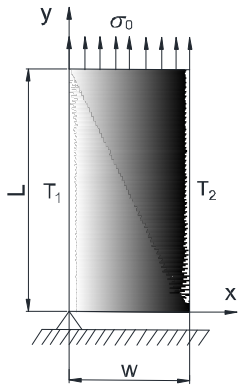

Figure 2: Boundary conditions of functionally graded plate

Property	Constituents	
	Ceramic ZiO_2	Metal Ti-6Al-4V
E, [Gpa]	117	66.2
υ	0.333	0.32
α, 10^{-6} [1/K]	7.11	10.3
k, [W/(mK)]	2.036	18.1

Table 1: Material properties of Ti-6Al-4V/ ZiO_2

The contour plots of the temperature field distributions as well as displacements and stress field with 11 x 21 node regular distributed. From Fig. 3a it can be seen that the temperature field is concentrated on the right side where rich ceramics are resistant to high thermal shock. Conversely, in Fig. 3b, the maximum value of the total displacement is concentrated in the top corner of the left face, where the metal is rich and able to withstand great pressure. It can also be seen from Fig. 3c that the tensile stress is concentrated mainly in the middle of the plate while the highest compressive stress occurs near the edges of the plate.

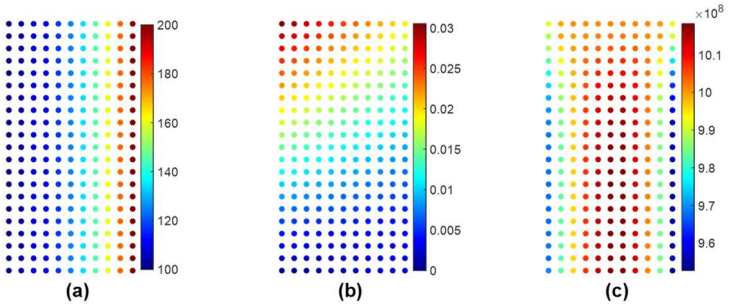

Figure 3: Numerical results computed by MATLAB with $\boldsymbol{\alpha_s = 1.3}$, $\boldsymbol{\eta = 4.001}$ for TPS shape function: (a)Temperature; (b) Total displacement; (c) Stress $\boldsymbol{\sigma_{yy}}$.

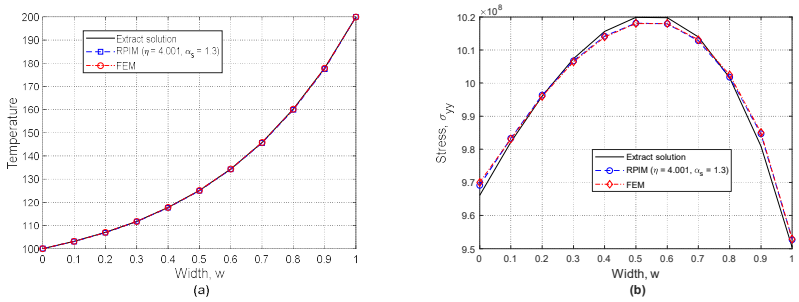

Figure 4: Comparison of the numerical approximations and the analytical solution along the y = 0 line: (a) Temperature; (b) Stress $\boldsymbol{\sigma_{yy}}$.

The temperature and stress distributions induced by the thermomechanical load are calculated continuously variable functionally graded materials using the exact solution, FEM and RPIM compared in Fig. 4a and 4b. All comparison graphs are presented along the line y = 0. Fig. 4a and 4b both show

quite excellent agreement between the results of the three methods. In Fig. 4b, the stress results between FEM and RPIM also have a high consistency, which is shown in the fact that the graphs coincide, the small difference between the two methods FEM and RPIM compared to the exact solution as shown in Fig. 4b can be explained by the finite length of the plate because for this problem mesh refinement does not bring a significant difference in results. These graphs have shown that the results in the RPIM are very consistent with both the FEM and the exact solution.

4.2 Hollow cylinder 2D FGM

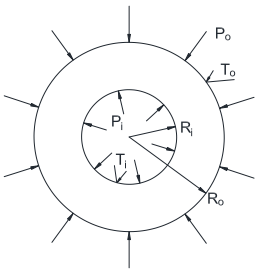

Figure 5: The cross-section of a graded hollow cylinder FGM.

Property	Constituents	
	Ceramic Al	Metal ZrO_2
E, [Gpa]	70.0	151.0
υ	0.3	0.3
α, 10^{-6} [1/K]	23.0	10.0
k, [W/(mK)]	204	2.09

Table 2: Material properties of Al/ ZrO_2

A hollow cylinder FGM with inner and outer radius $R_i = 1m$ and $R_o = 2m$, repectively in the plane strain state is considered is shown Fig. 5. Temperature conditions $T_i = 100K$ and $T_o = 200K$ are the temperatures at inner and outer surfaces of cylinder, while $P_i = 10^{12}$ and $P_o = 10^6$ units of pascal are the pressures on the inside and outside of the hollow cylinder, respectively. The material parameters are as shown in Table 2 are distributed with an exponential law in the radial direction.

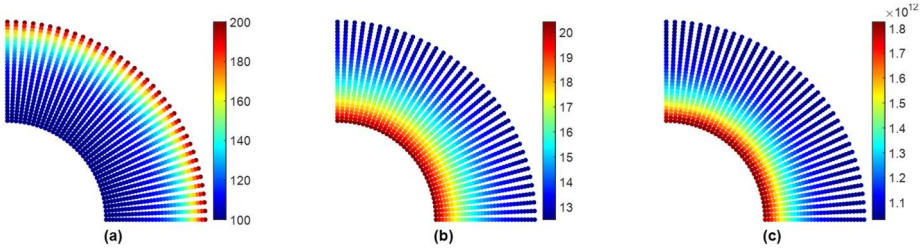

Figure 6: Numerical results computed by present method: (a) Temperature; (b) Total displacement; (c) Vonmises stress.

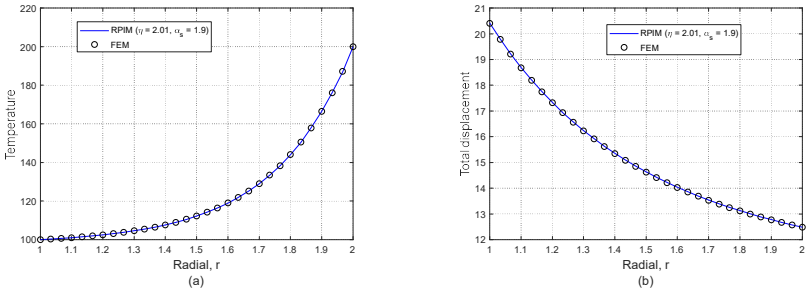

Figure 7: Comparison of approximation results in RPIM and FEM: (a) Temperature; (b) Total displacemnt

Due to the problem has symmetries in terms of boundary conditions, geometry and materials, we solve the problem on a quarter of the model. The results of temperature field distributions as well as displacements and stresses that are approximated by the present method will be compared and evaluated with the FEM approximation results by COMSOL Multiphysics software. Fig. 6 has shown the distribution of temperature field as well as displacement and stress fields approximated by RPIM under thermomechanical loads and corresponding corresponding boundary conditions as shown in Fig. 5.

The comparison graphs are presented along the x-axis of symmetry (y = 0) to evaluate in detail the results of the RPIM solution compared with the solution in COMSOL. Figure 7 shows that the temperature and displacement results in the present solution are accurate and completely consistent with the solution in COMSOL. The difference in the distribution of temperature and displacement in the two methods is almost unchanged when the number of field nodes changes. However, for the stress field, that is not the case so different numbers of nodes are applied to evaluate the variation of bias errors as well as the convergence of biases as shown in Fig. 10.

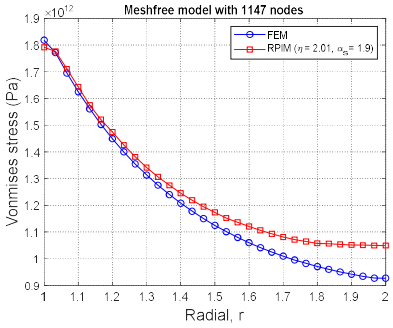

Figure 8: Comparison of vonmises stress between RPIM and FEM.

RPIM results		FEM results (COMSOL)		Error (%)
Node	Vonmises (GPa)	Element	Vonmises (GPa)	
42	1.4909	30	1.6694	10.6925
143	1.6650	120	1.7532	5.0308
304	1.7323	270	1.7845	2.9252
525	1.7632	480	1.8011	2.1043
806	1.7775	750	1.8114	1.8715
1147	1.7920	1080	1.8183	1.4464

Table 3: Stress error (%) between RPIM and FEM

Fig. 8 shows the difference in stress results between RPIM and FEM. The locations of stress concentration are the places to be concerned and the graph in Fig. 8 shows a pretty good agreement between the two solutions. That deviation is also presented in Table 3 for the different meshless models. The values there show a significant decrease in error as the number of nodes increases. The comparison graph, as well as the convergence rate of the errors, are shown in Fig. 9a and 9b respectively.

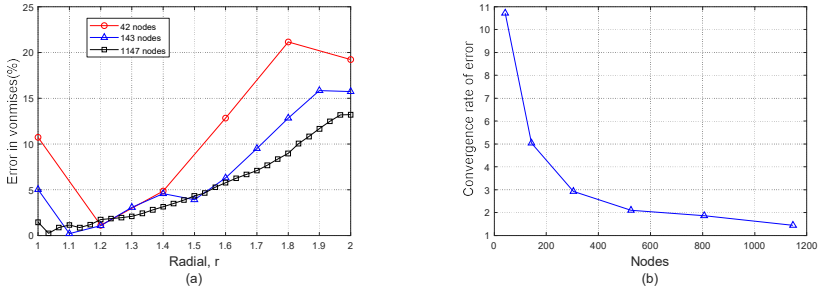

Figure 9: Error in vommise stress: (a) Error comparison; (b) Rate of convergence.

Fig. 10 shows the stress convergence rate of the RPIM compared with the FEM and shows that the convergence rate is quite good. Both have similar convergence speed, RPIM seems to be slightly faster. Therefore, it can be concluded that RIM can be effectively applied to this and other similar problems. Some other examples with more complex boundary conditions such as heat flux and convective heat

exchange will be solved by RPIM to further evaluate the effectiveness and applicability of the present method in many thermomechanical problems difference will be considered in the next section.

Property	Constituents	
	Ceramic Al	Metal SiC
E, [Gpa]	70.0	427
υ	0.3	0.17
α, 10^{-6} [1/K]	23.4	4.3
k, [W/(mK)]	233	65

Table 4: Material properties of Al/ SiC

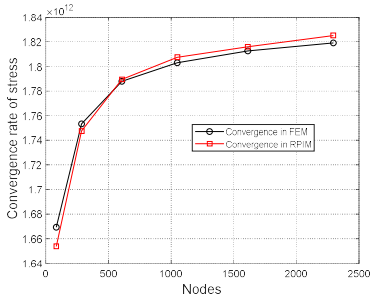

Figure 10: Convergence of Vonmises stress

4.3 Connecting rod FGM

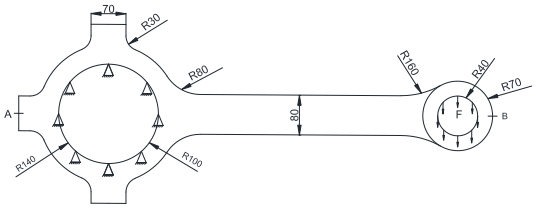

Figure 11: Geometrical sizes of connecting rod.

A connecting rod FGM has the basal geometrical size as shown in Fig. 11. The inner circular of connecting rod big end is fully constrained, and it is defined as subjected to a constant heat flux load $q_0 = 5.10^2\ W/m^2$. The inner circular of connecting rod small end is prescribed as constant heat flux load $q_1 = 10^2\ W/m^2$, and the uniform load acting on it is $10^7\ N/m^2$ in the direction shown in Fig. 11. The Robin convective boundaries are expressed by other edges with ambient temperature T_f=100K and convection heat transfer coefficient h=50 W/(m^2K). The material properties are assumed to vary in the x-direction according to the exponential with the material properties of ceramic and metal given as shown in Table 4.

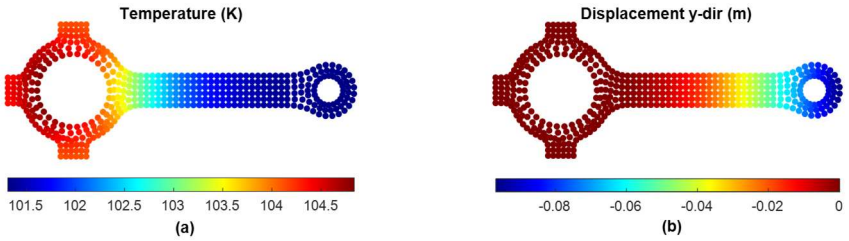

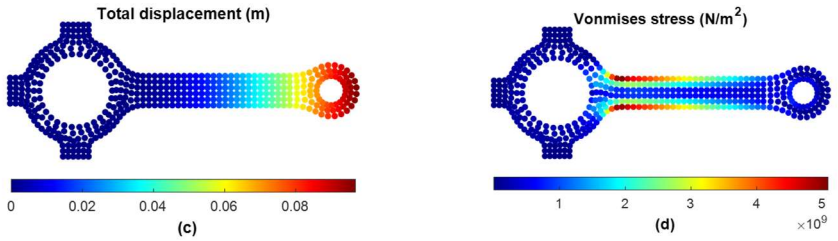

Figure 12: Approximate results of field functions using RPIM: (a) Temperature; (b) Displacement U_y; (c) Total displacement; (d) Vonmises stress

The RPIM calculation solution is validated by FEM since the analytic solution is not available. For effective comparison, the 351 element in FEM and 450 node in RPIM are used to discrete the computational domain. Fig.12 shows the distribution of field functions including temperature, displacement and stress field. Comparison graphs drawn on path AB including all edges from A to B.

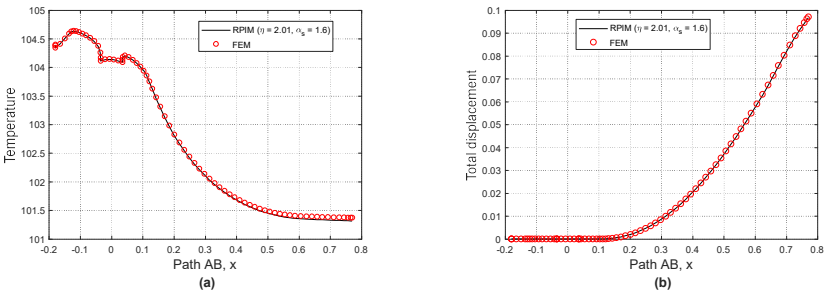

Figure 13: Compare the RPIM approximation with Comsol: (a) Temperature; (b) Total displacement

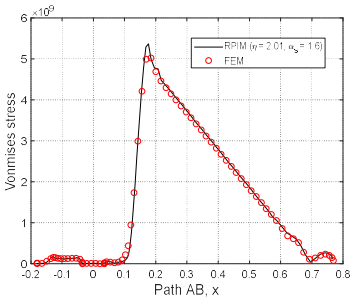

Figure 14: Comparison of vommises stress results between RPIM and FEM

RPIM results		FEM results (COMSOL)		Error (%)
Node	Vonmises (GPa)	Element	Vonmises (GPa)	
450	5.0839	351	5.0197	1.2790
784	5.2902	646	5.2662	0.4557
1103	5.3652	944	5.3722	0.1303

Table 5: Stress error (%) with different meshless models

Fig. 13 shows the good agreement of the temperature and displacement results obtained from the present method compared with COMSOL. In particular, the stress results in Fig. 14 also show that the results obtained in RPIM are really good, which is evidenced by the errors in Table 5.

5 Conclusions

In this paper, the RPIM method is applied to solve the thermomechanical problem for FGM materials. The programs are developed using the Matlab programming language. Through numerical examples, we can see that the solution obtained from this method is very consistent with the exact

solution and the results obtained from FEM even with quite complex and different types of boundary conditions. This proves that this is an effective method and high applicability of this method.

Acknowledgments

This research is funded by Ho Chi Minh City University of Technology (HCMUT), VNU - HCM under grant number SVCQ-2021-KHUD-03. We acknowledge Ho Chi Minh City University of Technology (HCMUT), VNU-HCM for supporting this study.

References

[1] O. C. Zienkiewicz, R. L. Taylor, The Finite Element Method: Volume 1: Basics, Elsevier, 2000.

[2] Tinh Quoc Bui, Dam Quang Vo, Chuanzeng Zhang, Du Dinh Nguyen, "A consecutive-interpolation quadrilateral element (CQ4): Formulation," *Finite Elements in Analysis and Design,* vol. 84, pp. 14-31, July 2014.

[3] Sahil Garg and Mohit Pant, "Meshfree Methods: A Comprehensive Review of Applications," *International Journal of Computational Methods,* vol. 15, no. 3, pp. 1-85, 17 October 2017.

[4] G. R. Liu and X. L. Chen, "A mesh free method for static and free vibration analysis of thin plates of arbitrary shape," *Journal of Sound and Vibration,* vol. 241, pp. 839-855, 2001.

[5] P. Krysl, T. Belytschko, "Analysis of thin plates by the element-free Galerkin method," *Computational Mechanics,* vol. 17, pp. 26-35, December 1995.

[6] H. H. P. Dao, "A Meshfree Radial Point Interpolation Method for Free Vibration of Laminated Composite Plates Analysis Based on Layerwise Theory," *Procedia Engineering,* vol. 142, pp. 349-356, 2016.

[7] Z. Kazemi, M.R. Hematiyan, R. Vaghef, "Meshfree radial point interpolation method for analysis of viscoplastic problems," *Engineering Analysis with Boundary Elements,* vol. 82, pp. 172-184, September 2017.

[8] J. G. Wang and G. R. Liu, "A point interpolation meshless method based on radial basis functions," *International Journal for Numerical Methods in Engineering,* vol. 54, pp. 1623-1648, 2002.

[9] Fuming Bao, Bingzhi Chen, Yanguang Zhao and Xinglin Guo, "An Improved 2D Meshfree Radial Point Interpolation Method for Stress Concentration Evaluation of Welded Component," *Applied Sciences,* vol. 10, pp. 1-17, 30 September 2020.

[10] G. R. Liu and Y. T. Gu, An Introduction to Meshfree Methods and Their Programming, Dordrecht, The Netherlands: Springer, 2005.

[11] H. K. Ching and S. C. Yen, "Meshless local Petrov-Galerkin analysis for 2D functionally graded elastic solids under mechanical and thermal loads," *Composites Part B: Engineering,* vol. 36, no. 3, pp. 223-240, April 2005.

[12] V.N. Burlayenko and et.al, "Modelling functionally graded materials in heat transfer and thermal stress analysis by means of graded finite elements," *Applied Mathematical Modelling,* vol. 45, pp. 422-438, 2017.

[13] F. Erdogan and B. H. Wu, "Crack problems in fgm layers under thermal," *Journal of Thermal Stresses,* vol. 19, no. 3, pp. 237-265, 1996.

[14] Wasim M. K. Helal and Dongyan Shi, "Optimum Material Gradient for Functionally Graded Rectangular Plate with the Finite Element Method," *Indian Journal of Materials Science,* vol. 2014, pp. 1-7, 17 February 2014.